Reports

Deep Current Measurements Suggest Long Waves in the Eastern Equatorial Pacific

Abstract. *During the 1975 El Niño expedition an array of conventional and electric field type near-bottom current recorders was deployed at the equator 300 kilometers west of the Galápagos Islands. While hydrographic observations were indicating El Niño activity off the South American coast, the current meters recorded an oscillation with a 25-day period, a wavelength of about 1000 kilometers, and an amplitude of 0.04 meter per second propagating westward at approximately 0.5 meter per second. These characteristics agree with theoretical models of a first-mode baroclinic Rossby wave trapped at the equator.*

Many large-scale, transient, oceanic phenomena, such as El Niño, Cromwell Current meanders, and the appearance and disappearance of the Somali Current may be caused by long-wave activity in the equatorial region. During the 1975 El Niño expedition, we deployed an array of near-bottom current meters and vertical electric field recorders to observe any equatorial long-wave activity which might be associated with an El Niño event.

In October 1974, Quinn (*1*) predicted an El Niño for early 1975, based on the atmospheric pressure difference (the southern oscillation index) between Easter Island and Darwin, Australia. This prediction motivated the El Niño expedition, intended to make observations within the region 2°N to 14°S and 95°W to the South American coast, in two cruises during February and March 1975 and April and May 1975, bracketing both the time and spatial extent of the predicted El Niño occurrence. Hydrographic observations during the first leg showed a massive transgression of warm, low-salinity water across the equator to 4°S, as well as a depression of the thermocline at the equator and along the coasts of Ecuador and Peru. Also the southeast trade winds at this time were unusually weak from 2°N to 10°S in the eastern Pacific, and it appeared that El Niño was actively developing. However, 2 months later during the second leg, observations depicted a drastic shift in oceanographic and meteorologic conditions back toward normalcy; the El Niño was short-lived (*2*).

The deep current meter array was deployed on 20 and 21 February 1975 and the instruments operated for about 2 months. Thus they sampled deep equatorial conditions just at the time that the El Niño development was actively progressing at the surface. Several investigators (*3–7*) have presented models of internal long waves caused by wind stress variations and have applied these models to El Niño. They show that wave motions arise rapidly in the equatorial zone (the *e*-folding time for a transient response is of the order of 1 month), and thus long-wave generation should be strong during an El Niño development period.

According to Godfrey (*4*), the wave generation mechanism begins with a slackening of the southeast trade winds, creating a Kelvin wave which travels eastward at 1 to 2 m/sec, causes downwelling at the eastern boundary, and consequently excites internal Rossby waves which are trapped at the equator. Thus the eastern equatorial boundary is a source of equatorially trapped Rossby waves which travel toward the west with a velocity

$$(gH)^{1/2}/(2M + 1), M = 1, 2, 3, \ldots$$

where g is gravitational acceleration, M is meridional mode number, and H is Lighthill's (*7*) "effective depth" for the first baroclinic mode, which equals 0.1 to 0.3 m for the eastern equatorial Pacific. Thus the fastest mode ($M = 1$) propagates westward at 0.3 to 0.6 m/sec.

An alternate source for long-wave generation has been suggested by Philander (*8*). His analysis indicates that instabilities in the equatorial current systems can also give rise to such long waves.

The instrument stations describe an equilateral triangle 110 km on a side, about 300 km west of the Galápagos Islands and centered on the equator (Fig. 1). In this region the water depth is about 3300 m and the bottom is characterized by irregularly spaced hills 30 to 90 m high. At each apex of the triangle, we moored a Scripps Institution of Oceanography free vehicle current meter (*9*) 10 m from the bottom and a University of Hawaii free vehicle vertical electric field recorder (*10*) which spans the bottom 1000 m of the water column. The current meter measures current speed and direction at the mooring location, whereas the electric field recorder yields the magnetic east-west component of velocity, averaged over the bottom 1000 m.

All instruments employed time releases set to trigger on 16 and 17 April 1975. However, the recovery ship, R.V. *Moana Wave*, experienced engine problems in early April and was unable to sail in time. We searched in vain for an alternate vessel until Admiral A. Arana of the Instituto del Mar del Peru ordered the R.V. *SNP-1* to divert from a coastal hydrographic cruise to pick up one of us (R.R.H.) and to proceed to the equatorial site. Despite a lack of navigational aids, the Peruvian investigators located and recovered the three current meters and one electric field recorder. All instruments operated for the full 2 months, except for the northernmost current meter (meter 1) which did not record at all. The records were digitized at 1-hour intervals and detided (that is, the tides were removed) by a low-pass filter.

Table 1. Time lags corresponding to maximum correlation between components.

Leading component	Lagging component	Lag (days)
Current meter 3, east-west	Current meter 2, east-west	2.9
Current meter 3, north-south	Current meter 2, north-south	2.5
Electric field	Current meter 2, east-west	0.3
Current meter 3, east-west	Electric field	2.8

Table 2. Possible wavelengths and velocity solutions for eastward- and westward-traveling waves.

Direction of waves	n	Wave-length L_n (km)	Velocity c_n (m/sec)
Westward propagation	0	1020	0.48
	1	100	0.04
	2	53	0.03
Eastward propagation	1	125	0.06
	2	59	0.03

Figure 2 shows the raw and detided current meter records in geomagnetic components for direct comparison with the electric field data, which are calibrated in velocity units. The tides and an oscillation with a period of about 25 days account for most of the observed energy. The 2-month recording at only two stations is insufficient to permit a proper statistical treatment of the 25-day oscillation, but we can estimate some characteristics of the wave.

Correlation between two records indicates their degree of similarity. We have computed the correlation as a function of lag so that the maximum correlation of a single component between two stations corresponds to the phase lag of the wave. Table 1 summarizes the optimum lags between components for the detided records. Both the north-south and east-west components of the current meters yield about 2½ days delay in traveling from station 3 to station 2. Following the reasoning of Düing *et al.* (*11*), for a wave with period (T) of 25 days, a distance (Δx) between stations of 111 km, and an average lag (ΔT) between stations of 65 hours, an infinite set of velocities (c_n) and wavelengths (L_n) are derived for eastward and westward traveling waves

$$c_n = \frac{\Delta x}{\Delta T + nT}, \quad n = 0, 1, 2 \ldots \quad \text{(westward)}$$

$$c_n = \frac{\Delta x}{nT - \Delta T}, \quad n = 1, 2 \ldots \quad \text{(eastward)}$$

Table 2 shows the first few possible solutions.

Although the available data do not allow us to distinguish between the possible solutions, the westward-propagating wave for $n = 0$ has characteristics which are consistent with theoretical results about the first-mode baroclinic Rossby wave. In particular, the phase speed of 0.48 m/sec is within the limits of 0.3 and 0.6 m/sec calculated by Godfrey (*4*) for the eastern Pacific. The wavelength, 1020 km, is smaller than the 2000 km estimated by Philander (*8*) for the Atlantic, but the 25-day period is roughly consistent with his result, 2 to 3 weeks. Moreover, Lighthill (*7*) calculated the energy partition in the Indian Ocean and concluded that most of the energy should reside in the first baroclinic mode, 7 percent as much in the barotropic mode, and < 1 percent as much in the higher baroclinic modes. White and McCreary (*3*) further reduced the ratio of barotropic to first baroclinic mode to 5 percent in the eastern equatorial Pacific.

Comparable experimental work has not been done in the Pacific, but both Düing *et al.* (*11*) and Meinke (*8*) have reported near-surface wave activity in the equatorial Atlantic. Meinke observed a wave with a 36-day period propagating westward at 0.5 m/sec with a wavelength of 1500 km. Düing *et al.* measured a wave with a 16-day period traveling to the west with a phase speed

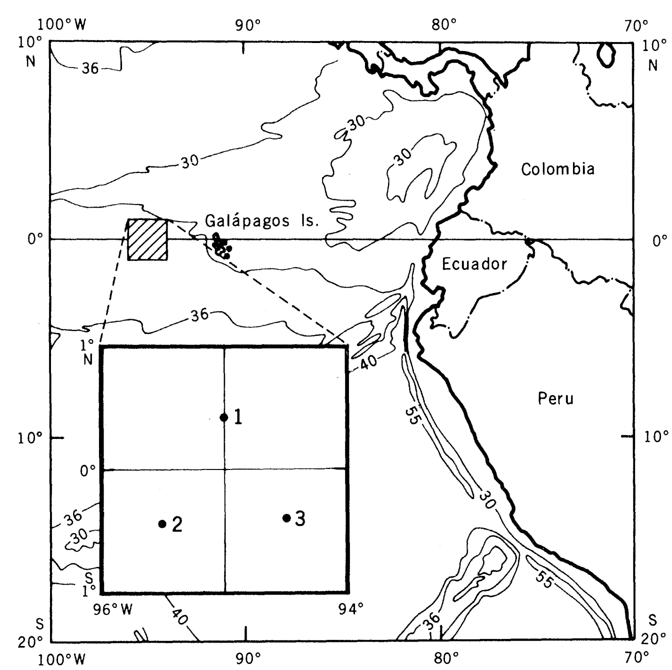

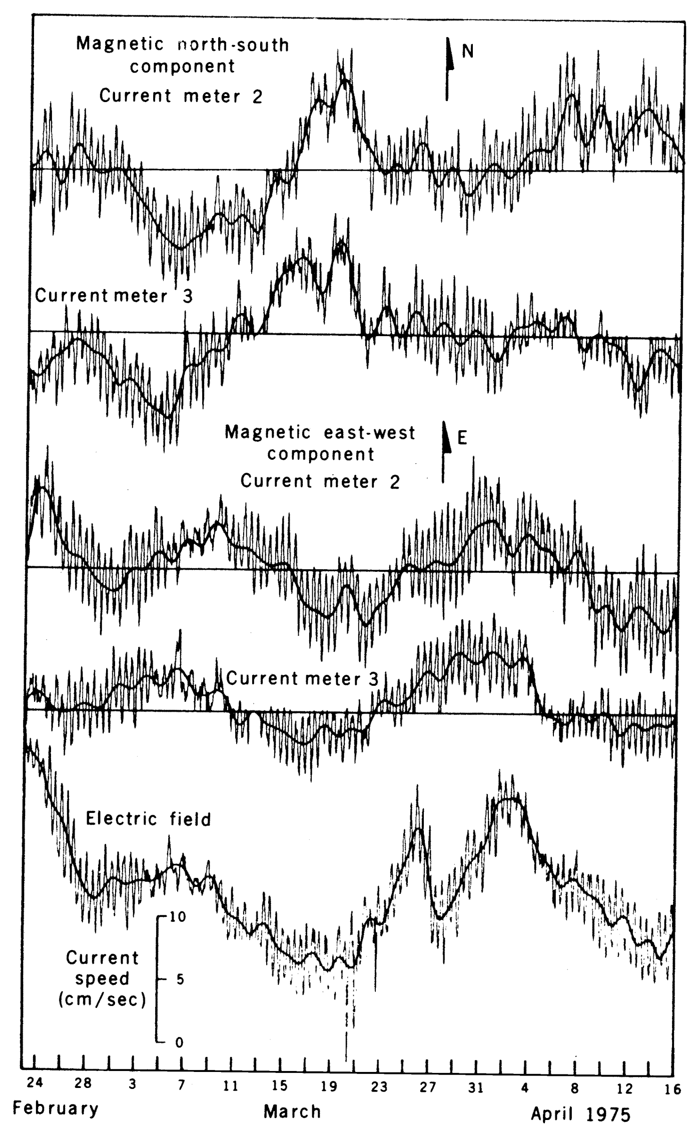

Fig. 1 (left). Locations of current recorders. Stations 1, 2, and 3 each included a bottom current meter and a recorder of vertical electric field over the bottom 1000 m. Depths are in hundreds of meters. Fig. 2 (right). Geomagnetic components of deep equatorial currents measured by current meters and an electric field recorder. The magnetic variation is 8°E. The darker, smoothed curves represent the detided records.

of 2.3 m/sec and a wavelength of 3200 km.

At one station Düing *et al.* noted that the disturbance occurred 3 to 4 days later at the surface than at a depth of 100 m. We also see this effect in comparing the electric field to the current meter data. Table 1 shows that the electric field, which represents the east-west transport averaged over the bottom 1000 m, lags the water current at meter 3, 10 m from the bottom, by 2.8 days and leads the current at meter 2 by 0.3 day, although the electric field recorder was located next to meter 3. However, the statistics of lag determinations are poor. Long observations from a larger array are needed to verify such a curious effect.

ROBERT R. HARVEY
Hawaii Institute of Geophysics, University of Hawaii, Honolulu 96822
WILLIAM C. PATZERT
Scripps Institution of Oceanography, La Jolla, California 92093

References and Notes

1. W. H. Quinn, *J. Appl. Meteorol.* 13, 825 (1974).
2. K. Wyrtki, E. Stroup, W. Patzert, R. Williams, W. Quinn, *Science* 191, 343 (1976).
3. W. B. White and J. P. McCreary, *J. Phys. Oceanogr.* 4, 295 (1974).
4. J. S. Godfrey, *ibid.* 5, 399 (1975).
5. J. P. McCreary, *ibid.*, in press.
6. R. H. Hurburt, J. C. Kindle, J. J. O'Brien, *ibid.*, in press.
M. J. Lighthill, *Philos. Trans. R. Soc. Lond. Ser. A* 265, 45 (1969).
8. The work of G. Philander and of J. Meinke is discussed in (*11*).
9. M. Sessions, *Exposure* 3, 1 (1975).
10. R. R. Harvey, *J. Geophys. Res.* 79, 4512 (1974).
11. W. Düing, P. Hisard, E. Katz, J. Meinke, L. Miller, K. V. Morashkin, G. Philander, A. A. Ribnikov, K. Voigt, R. Weisberg, *Nature (London)* 257, 280 (1975).
12. We want to thank K. Wyrtki for his permission to make the measurements during the El Niño expedition and Admiral A. Arana and the scientists and workers of the Instituto del Mar del Peru, without whose aid the instruments could not have been recovered. This research was sponsored by the Office of Naval Research under contract ONR 0014-70-A-0016-0001-AA, the National Oceanic and Atmospheric Administration under contract NOAA 05-6-022-51022, and the North Pacific Experiment (NORPAX). Hawaii Institute of Geophysics contribution No. 774.

22 March 1976; revised 23 June 1976

Inositol Isomers: Occurrence in Marine Sediments

Abstract. *A combined gas chromatographic–mass spectrometric technique was used to identify and quantitate the occurrence of* myo-, chiro-, *and* scyllo-*inositol in marine sediments. The most abundant isomer was* myo-*inositol. These inositols were found in all the organic-rich sediment samples examined, and the amount of inositol decreased steadily with the age of the sample. A small fraction of the inositols occurred as hexaphosphate esters.*

The inositols, the isomers of hexahydroxycyclohexane, occur in all higher organisms and most microorganisms (*1*). Of the nine possible stereoisomers, *myo*-inositol is generally the most abundant although *scyllo*-inositol may be the most abundant in sharks (*2*) and a certain red alga (*3*). The hexaphosphates of inositol, known as phytic acids, are also abundant, and up to 90 percent of the phosphate in some seeds and grain is in the form of phytic acids (*4*). As far as we know, free inositols have not been looked for in soils; however, complex mixtures of penta- and hexaphosphates (the isomers of *myo*-, D-*chiro*-, L-*chiro*-, *scyllo*-, *muco*-, and *neo*-inositol) have been found in soils (*5*, *6*), and unspecified phytic acid isomers have been found in lake water (*7*), where up to 50 percent of the total phosphorus is in the form of inositol phosphates (*7*, *8*). We report here the presence of three inositol isomers in marine sediments and show that a small portion of the inositols is in the form of phosphate esters.

Our analysis is based on the stability of inositols to hot HCl hydrolysis; under this treatment most other organic compounds including carbohydrates give insoluble, ionic, or volatile compounds (*9*). After filtration or centrifugation, the inositols are separated from the ionic species by ion-exchange columns which do not retain the inositols (*10*). Thus, 1- to 2-g (wet weight) samples of sediment (*11*) were hydrolyzed with 6*N* hydrochloric acid at 110°C for 48 hours. The insoluble material was removed by centrifugation and washed twice with water. The combined extracts were evaporated to dryness, dissolved in a minimal volume of water, and then applied to a double bed column of Dowex 50WX8 (H^+) and Dowex 2X10 (OH^-). After drying, the desalted eluent was silylated by treatment with a mixture of pyridine, hexamethyldisilazane, and trimethylchlorosilane (9 : 3 : 1) for 24 hours at room temperature.

The resulting silylated mixture was then examined directly by gas chromatography–mass spectrometry (GC-MS) (*12*). The trimethylsilyl (TMS) ethers of the nine stereoisomers separated on the column to give eight peaks (the enantiomers of *chiro*-inositol give only one peak) (*13*). The TMS ethers are excellent derivatives for the identification of the isomers of inositol since each TMS isomer produces a unique mass spectrum. The isomers yield identical ions, but the fragment intensities vary remarkably for stereoisomers (*14*).

The marine sediments assayed (Table 1) yielded only three major GC peaks, *myo*-, *chiro*-, and *scyllo*-inositol. The identifications are based on the mass spectra and GC retention times and on the results of coinjection with known inositol isomers. The quantitation of the inositol isomers was based on the GC peak heights and is accurate to ± 10 percent for the *myo*-inositol.

Control experiments in which the same procedure was used were carried out on sediment samples to which authentic inositol isomers had been added. The added inositols were recovered quantitatively. No interconversion of the isomers could be detected on acid hydrolysis in the presence or absence of the sediment. No inositols were found in water blanks or ignited sediment samples.

No inositols were extracted from the sediment samples after three extractions

Table 1. Content of *myo*-, *chiro*-, and *scyllo*-inositols in marine sediments in parts per million (ppm). The figures in centimeters refer to the depth in the core.

Sample and reference	Lithologic description	Time of deposition (years)	Inositols (ppm, dry weight)		
			myo-	*scyllo*-	*chiro*-
1, Santa Barbara Basin (*17*) (34°11.80′N, 120°02.00′W)	Coastal basin sediment	10	87	4.2	2.8
2, Santa Barbara Basin (*17*) (34°11.80′N, 120°02.00′W)	Coastal basin sediment	80	37	3.2	2.1
3, SOT W7 P12*, 15 to 30 cm (*18*) (2°35.00′N, 85°1.80′W)	Calcareous clay	5×10^4	3.1	0.14	0.10
4, 15-148-16-3†, 90 to 105 cm (*19*) (13°25.12′N, 63°43.25′W)	Calcareous clay	2×10^6	1.7	0.13	0.14
5, 36-328-3-6†, 0 to 15 cm (*20*) (49°48.67′S, 36°39.53′W)	Diatom-bearing clay	6×10^6	0.12	0.03	0.04
6, 15-146-36R-2†, 138 cm (*21*) (15°06.99′N, 69°22.67′W)	Foraminiferal limestone	45×10^6	0.03	0.009	0.010

*Scripps Institution of Oceanography core sample designation. †The numbers refer to Deep Sea Drilling Project numbers for leg-hole-core-section.